Journal of The Electrochemical Society, **152** (12) B534-B539 (2005)
0013-4651/2005/152(12)/B534/6/$7.00 © The Electrochemical Society, Inc.

Electrochemical Characterization of Pearlite Phase Oxidation of 1018 Carbon Steel in a Borate Medium using ECSTM Technique

Román Cabrera-Sierra,[a,b,*] Nikola Batina,[b,] and Ignacio González[b,**,z]**

[a]*Departamento de Metallurgia, Escuela Superior de Ingeniería Química e Industrias Extractivas (ESIQIE-IPN), C.P. 07738, México, D.F., Mexico*
[b]*Departamento de Química, Área de Electroquímica, Universidad Autónoma Metropolitana-Iztapalapa, C.P. 09340, México, D.F., Mexico*

The mechanism and progress of oxidation of the pearlite phase of 1018 carbon steel in contact with a borate medium was monitored and characterized using the in situ electrochemical scanning tunneling microscopy (ECSTM) technique. The pearlite phase was identified by characteristic microstructure using a previous experimental methodology. The progress of the pearlite oxidation due to differently imposed anodic potential was monitored via change of the electrode surface morphology. ECSTM images indicate two types of the iron oxide formation on the pearlite surface, with different and distinguished morphology. Regarding previously reported data about the oxide formation, these two types of iron oxides were associated to magnetite (internal oxide) and maghemite (external oxide). The needle-like features, as a genuine characteristic of the pearlite phase, are visible at the internal oxide layer and even at the maghemite layer. The cross-sectional analysis of the obtained images clearly shows detailed mechanism and morphology characteristics of the oxide layer development in both cases. Based on these observations, a detailed model of the pearlite surface modification during the oxidation was proposed. The model describes pearlite oxidation involving internally and externally formed iron oxides via several consecutive stages.
 [DOI: 10.1149/1.2109527]

Manuscript submitted January 21, 2005; revised manuscript received August 4, 2005. Available electronically October 24, 2005.

The corrosion process is one of the issues broadly discussed in the literature because of the huge economic losses it generates in different industrial applications. An alternative to corrosion problems is a use of highly resistant materials (i.e., alloys) that allow diminishing the corrosion rate of a substrate in contact with a corrosive medium. The anticorrosion properties of these materials is based on the existence of the passive film (surface metal oxide), which is highly resistant to the corrosive medium. Different physical models have been proposed in the literature to describe passivity of different metal substrates in contact with diverse aqueous media.[1-13] The most complete and best accepted is the point defect model (PDM) proposed by Macdonald et al.,[11-13] which is based on the description of passivity of different metal substrates considering diffusion processes of either cationic or anionic vacancies or interstitial metallic ions through the internally formed film (barrier layer).[13-16] As demonstrated in the literature, the PDM model also could be successfully used in the case of the bilayers, like oxides.[15] The inner oxide layer (near to the substrate), with homogeneous and passive properties was identified as barrier layer; meanwhile, the external film is nonhomogeneous with poor passive properties. The external film is formed due to transformation (oxidation) of the barrier layer through a solid-state reaction.[15,17-21] The chemical composition of metal oxides has been established reliably for different metal-neutral aqueous medium interfaces, i.e., valve materials.[22-24]

In particular, for the iron/aqueous solution interface, the barrier layer has been associated to magnetite (Fe_3O_4), and the nonhomogeneous outer layer, with nonpassive properties, to maghemite (γ-Fe_2O_3).[19-21] This previous information has been considered in this paper in order to correlate the observed changes in the surface morphology detected by electrochemical scanning tunneling microscopy (ECSTM) during the carbon steel surface oxidation process in borate aqueous solution. In our study, due to the different phases (microstructures) present in the carbon steel[25], one in the iron-rich region, ferrite (Fe-α), and the second consisting of an alternate arrangement of ferrite and iron carbide (cementite, Fe_3C) that is part of the pearlite phase, everything is rather complex. Especially when one takes into consideration that the oxidation mechanisms of these microstructures could be different as well as the function of their structure and metallographic characteristics.[25,26]

Thus, the objective of this work was to study the oxidation mechanism of the pearlite phase, as a specific segment of the 1018 carbon steel surface, directly in a borate medium using ECSTM at real-time. Such an approach, based on the local observation, limited on the selected segment of the real sample surface, so far was not explored, as we know. Therefore, we believe that ECSTM characterization in these conditions could provide valuable information about different mechanisms of the oxide formation at the carbon steel materials, which also could lead to new applications.

Experimental

Preparation of the working medium.— The electrolyte media used in this study were prepared with suprapure water (18.2 MΩ cm) (Millipore), and analytic grade reagents from Merck, including borate buffer (pH 7.8) (prepared by mixing a solution of 0.642 M H_3BO_3 and 0.1 M sodium hydroxide).

Sample preparation.— The working electrode was a 1018 carbon steel disk with the typical composition of: 0.14–0.20% C, 0.60–0.9% Mn, 0.035% max. S, 0.030% max. P, and the rest Fe. The electrode was cleaned by polishing the steel with 400 and 600 silicon carbide emery papers until obtaining a homogeneous surface. A mirror finish was obtained using a piece of cloth and 0.3-μm particle-sized alumina. Finally, samples were rinsed with acetone and water.

Equipment used.— ECSTM studies were performed using a scanning tunelling microscope (STM) from Molecular Imaging with a Picostat (bipotentiostat) adapted to an electrochemical cell (in situ mode). An STM electrochemical cell was made of Teflon with exposed sample area of 0.33 cm^2. Platinum and copper oxide/copper wires were used as a counter and pseudo reference electrodes, respectively. The pseudo reference electrode (Cu_2O/Cu [27]) showed a great stability in the borate medium with a constant potential of 0.140 V vs a normal hydrogen electrode (NHE). All potentials presented in this work are quoted with respect to the NHE. STM tips were prepared by electrochemical etching of tungsten wire in a 6 N NaOH solution and covered with nail polish.[28] The usual imaging conditions were a bias potential of −0.18 V and a set-point current of 2–3 nA. ECSTM images were recorded both after introducing the

* Electrochemical Society Active Member.
** Electrochemical Society Student Member.
z E-mail: igm@xanum.uam.mx

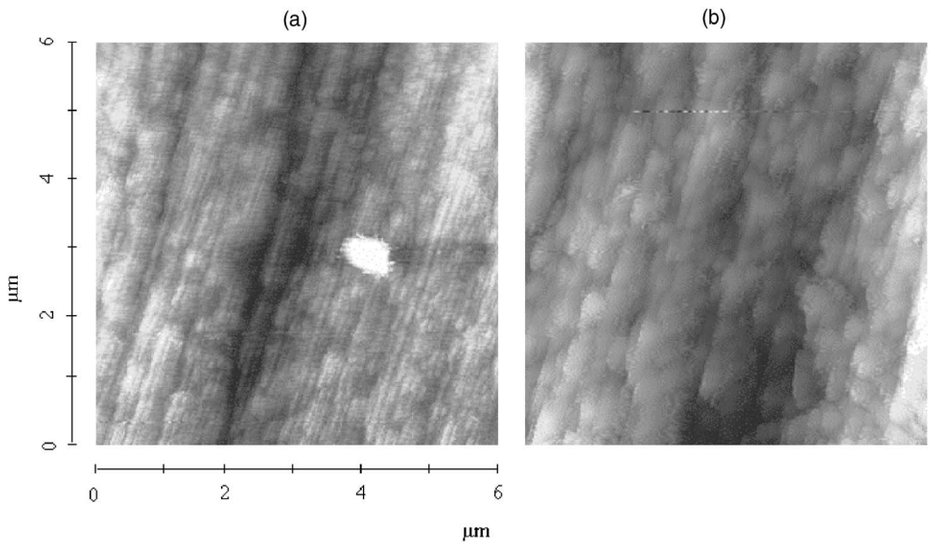

Figure 1. Typical ECSTM images (6 × 6 μm) of the pearlite structure obtained on 1018 carbon steel surface immersed in the borate medium (pH 7.8), after different immersion times: (a) 11.5 min (Z scale: 0–275 Å) and (b) 84 min (Z scale: 0–225 Å).

solution or imposing different anodic potentials while the tip was in the tunneling mode and scanned over the same area of the sample. In this way the observed surface topography changes are assigned to the same electrode region. Studies were repeated several times, always with freshly prepared electrodes.

Results and Discussion

Identification of the pearlite phase, as a constituent of the 1018 carbon steel, in a borate medium using ECSTM.— ECSTM images presented in Fig. 1 were obtained using the previously developed experimental methodology proposed in our previous work[26] based on identification of the pearlite phase of 1018 carbon steel in a borate medium using the ECSTM technique. As shown at images in Fig. 1, the key issue is the identification of periodical arrangement characteristic for the pearlite phase (Fig. 1a) and monitoring its evolution (morphology) with the immersion time (Fig. 1b) without external potential applied.

Surface structures visualized in these images are characteristic for the low oxidized pearlite phase. It shows an alternate arrangement of ferrite (Fe-α) and iron carbide (FeC_3), which modifies its oxidation in the corrosive medium. As known from the previous SEM studies,[29,30] the line features on the carbon steel surface are related to the characteristic microstructure of pearlite.[29,30] Note, the surface structure observed in our ECSTM images is similar, identical to one previously found by SEM. The distances between the observed line, features in SEM (0.095 μm) and STM images (0.1 μm), are the same. Therefore it could be concluded that the particular segment probed by ECSTM is pearlite.

Figure 1b shows an example of the pearlite surface after the early stage of oxidation, without external potential applied. The obtained images show that the oxide layer grows along the lamellar pearlite phase, maintaining the pearlite periodical arrangement. The image presented in Fig. 1b was obtained 84 min after the sample immersion in the solution (no external electrode potential was applied). The fact that the image revealed the surface oxide formation leads to the conclusion that in such conditions, no oxide-free surface could be maintained and observed.

The pearlite phase oxidation in borate medium (internal oxide formation).— Figure 2 shows a different set of images obtained at the start of characterization of 1018 carbon steel in a borate medium using the ECSTM technique (image size: 6 × 6 μm). The surface morphology characteristics in these particular images are slightly different than those presented in Fig. 1 due to shorter time of immersion (8–10 min). However, it is clear by surface features that images on Fig. 2 also show the pearlite structure. Figures 1b and 2b

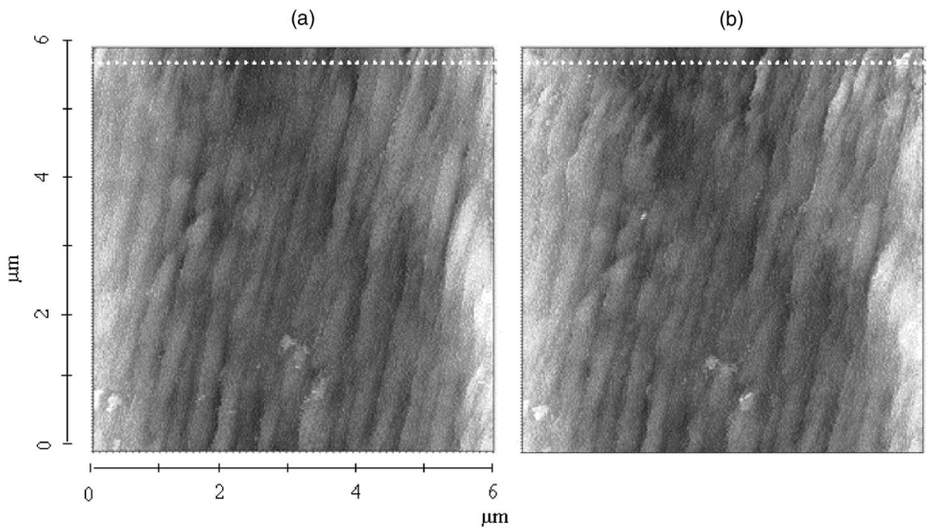

Figure 2. ECSTM images (6 × 6 μm, Z scale: 0–180 Å) of the pearlite structure obtained on 1018 carbon steel in borate medium (pH 7.8), without imposing the oxidation potential to the electrode interface. The images were obtained after (a) 8 and (b) 10.5 min.

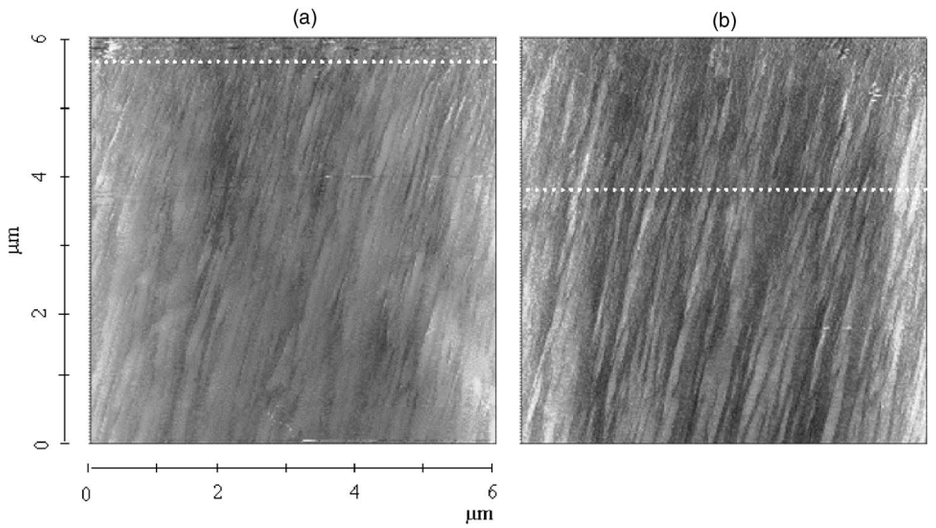

Figure 3. ECSTM images (6 × 6 µm, Z scale 0–295 Å) of the pearlite surface recorded after applying the oxidation potential of −0.120 V vs NHE. Images were obtained (a) at the beginning (3.33 min) and (b) at the end of the oxidation treatment (33.33 min).

show an oxidized pearlite surface due to immersion, without applied external potential. We found that the sample oxidation process takes place at the corrosion potential (open-circuit potential) of −0.125 V vs NHE.[26] Images show changes in the electrode morphology and the surface feature remains essentially unchanged, indicating the surface oxide formed is homogeneous and suggesting formation of the internal oxide (barrier layer). In accordance to the previous studies,[11-16] this film could be adherent with passive properties and clearly it can be characterized as magnetite.[19-21] These particular images on Fig. 1b and 2b, of the internally formed iron oxide layer, are reference for our further evaluation of the oxidation process and are compared and discussed in terms of nature of an iron oxide externally formed.

The pearlite phase oxidation in borate medium (external oxide formation).— To study further progress of the oxidation of the pearlite phase in a borate medium, the oxidation potential was applied at the electrode surface and changes in the surface morphology were monitored. This strategy allows us to reveal a probable mechanism of local oxidation at particular microstructures and also to identify the formation of corrosion products at the surface. Furthermore, the oxide growth characteristics at the steel surface can be evaluated in light of the above-mentioned bilayer model.[19-21]

Because this work intends to study the way in which the oxidation mechanism of pearlite phase initiates and to distinguish the iron oxide formation at the surface, the oxidation potentials selected and applied are very close to the corrosion potential. Since the bias potential used to obtain the images considers the tip and sample potentials, the potential range used for sample oxidation is not likely to cause a considerable change in the quality of the STM images.

Figure 3 shows typical images obtained by imposing an external potential of −0.120 V vs NHE (overpotential 5 mV) at a period of 33.33 min. The image at Fig. 3a shows the surface morphology for a sample oxidized during a short oxidation time of 3.33 min, and the image at Fig. 3b shows the surface morphology of the sample after 33.33 min. During the imposed potential, a slight anodic current of 0.6 µA was observed, possibly due to modification of the morphology of the inner oxide layer (magnetite) shown previously in Fig. 2b.

Analyzing images at Fig. 3 and comparing with images on Fig. 1 and 2, one could see that during the short oxidation period (imposed oxidation potential), at the early stages of the oxidation, the original laminar arrangement of the pearlite phase is still visible, preserved. However the rugosity of the sample surface seems to increase. The new oxide preferentially grows at the top of the magnetite/pearlite lines, or the oxide layer morphology and the oxide layer growth are determinated by the initial pearlite structure. The formation of such preferential growth is mostly related to the rapid oxidation (maghemite formation) of the ferrite component. On the contrary, as expected from the literature data,[25] oxidation of the cementite phase is slower.

In order to follow the oxide development one could analyze changes in the electrode surface morphology presented by cross sections of the ECSTM images (Fig. 4). Analysis starts with comparison of the morphology of magnetite oxide (internally formed without applied potential, Fig. 4a, taken from image on Fig. 2b) and the initial maghemite oxide layer (applied electrode potential −0.120 V,

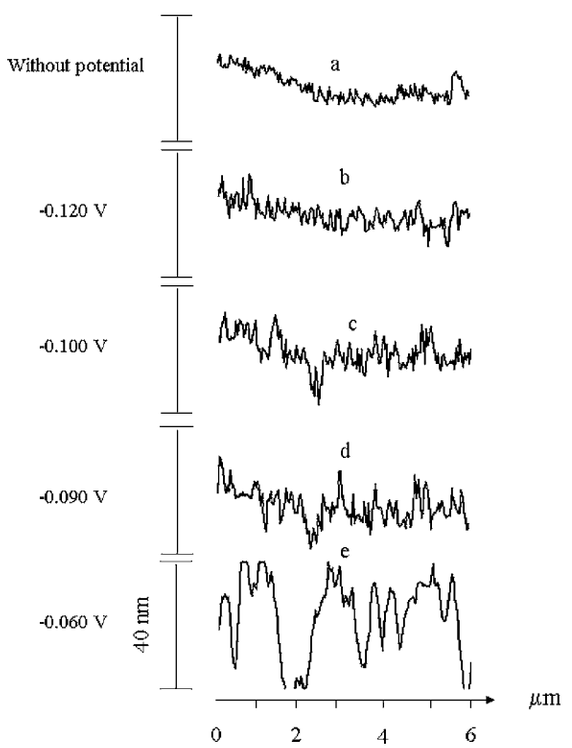

Figure 4. Cross-sectional analysis of the images of the pearlite surface obtained during progress of the oxidation process. Images were recorded (a) at the open-circuit potential (−0.125 V) and at different potentials imposed to the electrode interface: (b) −0.120, (c) −0.100, (d) −0.090, and (e) −0.060 V vs NHE.

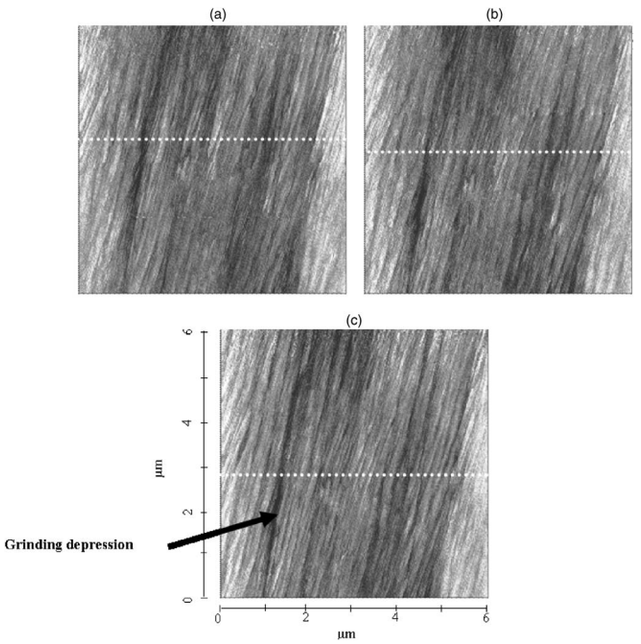

Figure 5. Typical ECSTM images (6 × 6 μm, Z scale 0–275 Å) of the oxidized pearlite surface recorded after applying a potential of −0.090 V vs NHE. The images were obtained in the borate medium (pH 7.8) (a) at the beginning (3.33 min), (b) after 10 min, and (c) at the end of the oxidation treatment (16.66 min). Dotted lines show location of the cross-sectional analysis.

Fig. 4b, taken from Fig. 3b). Despite similarities in appearance of the pearlite type of needle-shaped periodical arrangement, it is clearly visible that the maghemite layer possesses higher corrugation. By further progress of the oxidation (potential or time of oxidation), the maghemite layer becomes thicker and more corrugated (Fig. 4c-e). The analysis shown in Fig. 4 was evaluated from images obtained at the following oxidation potentials: without (a), −0.120 V (b), −0.100 V (c), −0.090 V (d), and −0.060 V (e) vs NHE. All cross-sectional data were plotted within the same Z scale for easier comparison.

Figure 5 shows images obtained during a longer period of time when an oxidation potential of −0.090 V vs NHE was applied. Note the applied potential is close to the open-circuit potential of the used sample. Progress of oxidation can be monitored at Fig. 5a-c after 3.33, 10, 16.66 min, respectively. Images clearly revealed that surface morphology changes in dependence of the time of oxidation. Note changes in the distances between the linear structures and especially an appearance of a grinding depression at the left side of the image. Taking into account the earlier literature reports about behavior of the iron substrate in a borate medium,[19-21] which established that the use of oxidation potentials near corrosion potential can result in a dissolution of potentiostatically formed iron oxides, we believe that observed changes in the maghemite surface morphology are a product of the selective growth and dissolution of the surface oxide as two competitive processes. In this way it is worth noticing that these images are probably the first sequences of such a process ever recorded.

Note that the observed phenomenon was limited at a certain potential range between −0.090 and −0.070 V vs NHE. In the case of imposing a potential of −0.060 V (slightly out of the mentioned range), the oxide growth becomes predominant in comparison to the dissolution process, and the electrode surface becomes rough with larger corrugation, as shown in Fig. 6. At the same time we also noticed that the image quality decreases, which could be related to rapid formation of the thick layer of maghemite layer (known to lower conductivity).[20] At positive oxidation potentials, as demonstrated in Fig. 4e, the predominant growth of the oxide layers leads to overall increase of the oxide thickness.

The observed behavior allows us to propose some kind of general mechanism for the oxide growth on the pearlite surface. First, the internallly formed oxide layer, magnetite, possesses similar structure as the pearlite substrate (typical ridge features). The externally formed oxide layer, maghemite, is different, with small needle-like features revealed by STM. Besides a different shape of features observed in STM images, one also could say that during the formation of the maghemite, the surface becomes rougher. Figure 7 shows a scheme of the proposed mechanism of electrochemically induced oxidation of a pearlite microstructure in contact with an aqueous solution of borates. The first stage of this mechanism considers the presence of a pearlite phase with characteristic and well-defined ridges due to alternate ferrite/cementite arrangement (stage 1). An immediate interface oxidation of ferrite component, due to contact with corrosive medium (even without applied oxidation potential), induces change in the surface morphology of the pearlite surface (increase of the ridge height) (stage 2). This part essentially describes the formation of the magnetite oxide layer. When anodic oxidation potential is imposed, the electrode surface morphology

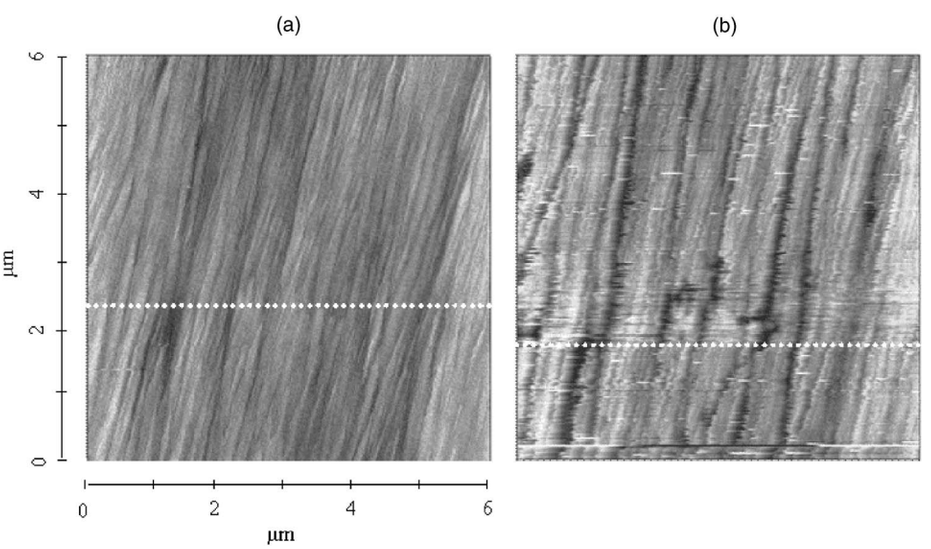

Figure 6. Typical ECSTM images (6 × 6 μm, Z scale 0–500 Å) of the oxidized pearlite surface recorded after applying a potential of −0.060 V vs NHE. The images were obtained in the borate medium (pH 8.4) (a) at the beginning during the first 3.33 min and (b) at the end of the oxidation (10 min).

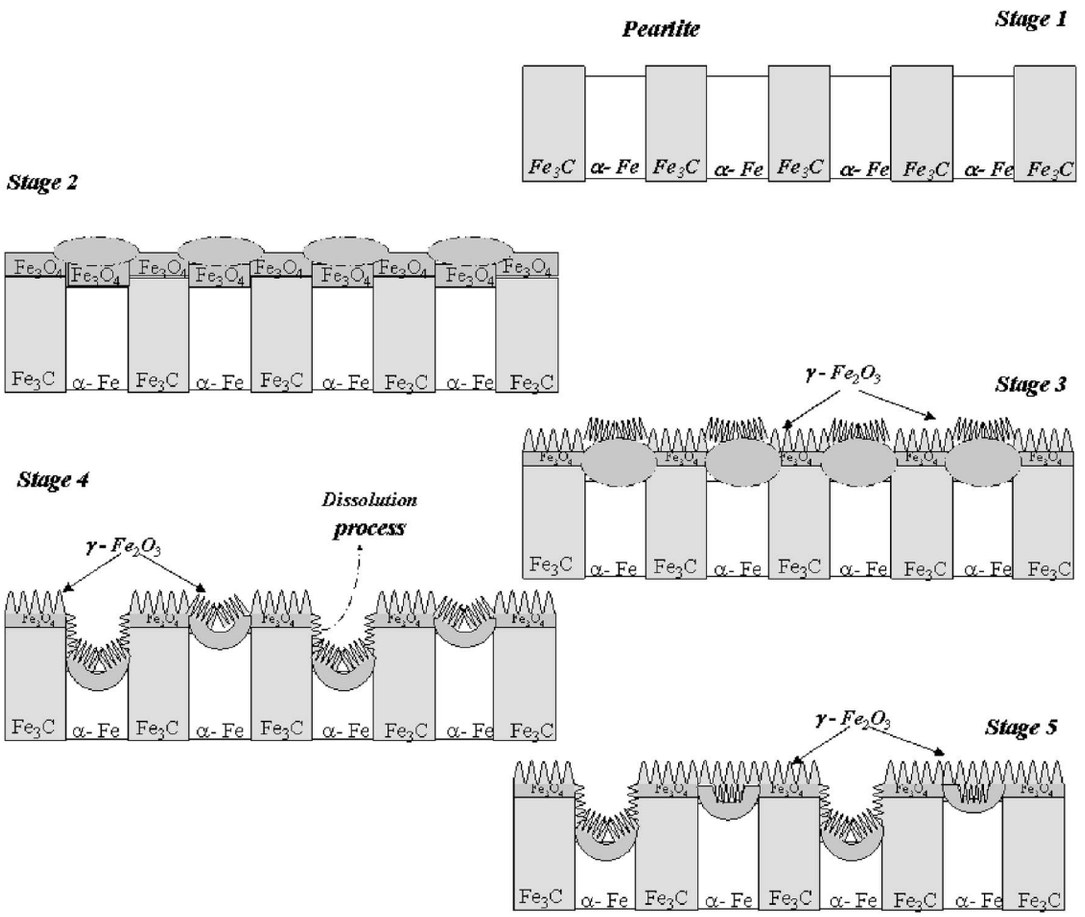

Figure 7. Schematic representation of the pearlite oxidation mechanism, in the aqueous solution of borates, showing different stages of the oxide formation in respect to the local composition of the pearlite surface.

changes drastically, at micro and macroscopic level, due to several possible reasons. First, it is due to predominant and rapid oxidation of ferrite, as illustrated in stage 3. It is followed by slow oxidation of a cementite surface and formation of the external maghemite oxide layer. At the early stages of the maghemite formation, the oxide growth and dissolution are competitive processes, which results in development of the high rugosity of the oxide surface (stage 4). However, when the oxidation potential increases toward more positive values (more than −0.070 V), development of the thick externally formed oxide is a predominant process (stage 5).

Conclusions

The oxidation mechanism of the pearlite phase of 1018 carbon steel in contact with a borate medium using the ECSTM technique was studied and characterized in detail. The initial point of our study was identification of the pearlite phase on the basis of the specific microstructure and its stability during prolonged time of contact with corrosive solution. In order to proceed with the oxidation process, an electrochemical treatment was imposed using different oxidation potentials, and surface morphology was monitored continuously (in situ ECSTM). Revealed images suggested a specific mechanism involving formation of two iron oxides on the pearlite: the internally formed magnetite and externally formed maghemite, which is in accordance with previously reported findings.[19-21] We found that oxide growth is coordinated by the initial structure of the pearlite phase. The needle-like features, as genuine characteristics of the pearlite phase, are visible at the internal oxide layer and even at the maghemite layer. Analysis of the cross sections at the obtained images shows an increase of the thickness and corrugation as a function of the applied potential. However, in the potential region between −0.090 and −0.070 V, an interesting phenomenon was observed, involving two competitive processes of the oxide growth and oxide dissolution. At more positive potentials the oxide growth becomes a predominant process. Progress of the pearlite oxidation was monitored by change of the surface morphology. Based on these observations, a detailed model of the pearlite surface modification during the oxidation was proposed. The model describes pearlite oxidation involving internally and externally formed iron oxides via several consecutive stages.

Acknowledgments

R.C.-S. is grateful to CONACYT for his Ph.D. scholarship and COTEPABE-IPN for the academic support. Financial support for N.B. was provided by Instituto Mexicano del Petróleo (IMP), project FIES-98-100-I. I.G. acknowledges financial support from CONACYT project 47162.

Universidad Autonoma Metropolitana-Iztapalapa assisted in meeting the publication costs of this article.

References

1. N. Cabrera and N. F. Mott, *Rep. Prog. Phys.*, **12**, 163 (1948).
2. L. Young, *Can. J. Chem.*, **37**, 276 (1959).
3. N. Sato and M. Cohen, *J. Electrochem. Soc.*, **111**, 512 (1964).
4. R. D. Armstrong and K. Edmondson, *Electrochim. Acta*, **18**, 937 (1973).
5. R. Kirchheim, *Electrochim. Acta*, **32**, 1619 (1987).
6. R. Kirchheim, *Corros. Sci.*, **29**, 183 (1989).
7. K. Noda, T. Tsuru, and S. Haruyama, *Corros. Sci.*, **31**, 673 (1990).
8. C. V. D' Alkaine, L. M. M. De Souza, and F. C. Nart, *Corros. Sci.*, **34**, 129 (1993).
9. E. B. Castro, *Electrochim. Acta*, **39**, 2117 (1994).

10. M. Bojinov, G. Fabricius, T. Laitinen, K. Mäkelä, T. Saario, and G. Sundholm, *Electrochim. Acta*, **45**, 2029 (2000).
11. C. Y. Chao, L. F. Lin, and D. D. Macdonald, *J. Electrochem. Soc.*, **128**, 1187 (1981).
12. D. D. Macdonald and M. Urquidi-Macdonald, *J. Electrochem. Soc.*, **137**, 2395 (1990).
13. D. D. Macdonald, S. R. Biaggio, and H. Song, *J. Electrochem. Soc.*, **139**, 170 (1992).
14. L. Zhang, D. D. Macdonald, E. Sikora, and J. Sikora, *J. Electrochem. Soc.*, **145**, 898 (1998).
15. J. Liu and D. D. Macdonald, *J. Electrochem. Soc.*, **148**, B425 (2001).
16. D. D. Macdonald, K. M. Ismail, and E. Sikora, *J. Electrochem. Soc.*, **145**, 3141 (1998).
17. I. Diéz-Pérez, P. Gorostiza, F. Sanz, and C. Müller, *J. Electrochem. Soc.*, **148**, B307 (2001).
18. J. Li and D. J. Maier, *J. Electroanal. Chem.*, **454**, 53 (1998).
19. M. Nagayama and M. Cohen, *J. Electrochem. Soc.*, **109**, 781 (1962).
20. A. J. Davenport and M. Sansone, *J. Electrochem. Soc.*, **142**, 725 (1995).
21. L. J. Oblonsky, A. J. Davenport, M. P. Ryan, H. S. Isaacs, and R. C. Newman, *J. Electrochem. Soc.*, **144**, 2398 (1997).
22. N. Casillas, S. Charlebois, W. H. Smyrl, and H. S. White, *J. Electrochem. Soc.*, **141**, 636 (1994).
23. S. B. Basame and H. S. White, *Langmuir*, **15**, 819 (1999).
24. C. J. Boxley, H. S. White, C. E. Gardner, and J. V. Macpherson, *J. Phys. Chem. B*, **107**, 9677 (2003).
25. *Properties and Selection: Iron and Steel*, Vol. 1, *Materials Characterization*, Vol. 10, J. R. Davies, Editor, American Society of Metals (ASM), Materials Park, OH (1986).
26. R. Cabrera-Sierra, N. Batina, and I. González, *Mater. Chem. Phys.*, In press.
27. V. Maurice, H. H. Strehblow, and P. Marcus, *J. Electrochem. Soc.*, **146**, 524 (1999).
28. N. Batina, T. Yamada, and K. Itaya, *Langmuir*, **11**, 4568 (1995).
29. D. G. Enos and J. R. Scully, *Metall. Mater. Trans. A*, **33A**, 1151 (2002).
30. S. W. Thompson and P. R. Howell, *J. Mater. Sci. Lett.*, **17**, 869 (1998).